

Diffusion Tensor Tractography of the Brainstem Pyramidal Tract: A Study on the Optimal Reduction Factor in Parallel Imaging

뇌간 추체로의 확산텐서 신경다발 영상: 병렬 영상에서의 적정 감소 인자에 대한 연구

Yun Jung Bae, MD, Jong Bin Park, BS, Jae Hyoung Kim, MD*,
Byung Se Choi, MD, Cheolkyu Jung, MD

Department of Radiology, Seoul National University College of Medicine, Seoul National University Bundang Hospital, Seongnam, Korea

Purpose: Parallel imaging mitigates susceptibility artifacts that can adversely affect diffusion tensor tractography (DTT) of the pons depending on the reduction (R) factor. We aimed to find the optimal R factor for DTT of the pons that would allow us to visualize the largest possible number of pyramidal tract fibers.

Materials and Methods: Diffusion tensor imaging was performed on 10 healthy subjects at 3 Tesla based on single-shot echo-planar imaging using the following parameters: b value, 1000 s/mm²; gradient direction, 15; voxel size, 2 × 2 × 2 mm³; and R factors, 1, 2, 3, 4, and 5. DTT of the right and left pyramidal tracts in the pons was conducted in all subjects. Signal-to-noise ratio (SNR), image distortion, and the number of fibers in the tracts were compared across R factors.

Results: SNR, image distortion, and fiber number were significantly different according to R factor. Maximal SNR was achieved with an R factor of 2. Image distortion was minimal with an R factor of 5. The number of visible fibers was greatest with an R factor of 3.

Conclusion: R factor 3 is optimal for DTT of the pontine pyramidal tract. A balanced consideration of SNR and image distortion, which do not have the same dependence on the R factor, is necessary for DTT of the pons.

Index terms

Diffusion Tensor Imaging
Magnetic Resonance Imaging
Pons
Pyramidal Tracts
Signal-To-Noise Ratio

Received August 6, 2015

Revised November 13, 2015

Accepted January 17, 2016

*Corresponding author: Jae Hyoung Kim, MD
Department of Radiology, Seoul National University
College of Medicine, Seoul National University
Bundang Hospital, 82 Gumi-ro 173beon-gil, Bundang-gu,
Seongnam 13620, Korea.
Tel. 82-31-787-7602 Fax. 82-31-787-4011
E-mail: jaehkim@snu.ac.kr

This is an Open Access article distributed under the terms of the Creative Commons Attribution Non-Commercial License (<http://creativecommons.org/licenses/by-nc/3.0>) which permits unrestricted non-commercial use, distribution, and reproduction in any medium, provided the original work is properly cited.

INTRODUCTION

Parallel magnetic resonance imaging (MRI) techniques have been widely utilized to shorten scan times or improve spatial resolution (1, 2). Parallel imaging reduces the number of phase-encoding steps by a reduction (R) factor, which refers to the ratio of original phase-encoding steps to reduced phase-encoding steps. The R factor ranges from 1.5 to 4 in most commercially available applications (1, 2). Although applications with much higher R factors are possible, they are currently limited by poor signal-

to-noise ratio (SNR) and image reconstruction artifacts (1-3).

The use of diffusion tensor tractography (DTT) of the cerebral white matter has become widespread in research into a broad spectrum of diseases (4-6). DTT is an imaging method based on diffusion weighted imaging data, which is usually obtained by single-shot echo-planar imaging (EPI). Single-shot EPI has several inherent drawbacks, including low SNR and vulnerability to susceptibility artifacts (1, 2). These drawbacks can be partially overcome by parallel imaging; the reduction in phase-encoding steps increases the SNR via a reduction in the echo time

(TE) (7, 8) and decreases the susceptibility artifact through a reduction in the phase error (3, 9). Shortening of the TE by parallel imaging in EPI can increase the SNR, in contrast to spin-echo or turbo spin-echo imaging, in which the SNR decreases proportionally to the square root of the R factor. In a previous study (7), the SNR of EPI increased with R up to the range of 2–3, and thereafter declined because the image reconstruction artifact of the parallel imaging process became dominant. On the other hand, susceptibility-induced geometric distortion in EPI decreased continuously with increasing R factor because the phase error of EPI is inversely proportional to the R factor (10).

The susceptibility artifact of EPI is pronounced at the pons-sphenoid interface and causes severe geometric image distortion, particularly at 3 Tesla, although this artifact can be mitigated by the use of parallel imaging (10, 11). Recently, many studies have emphasized a diagnostic role for DTT in brainstem imaging, particularly in cases of tumorous disease (12–15). However, susceptibility-induced geometric distortion at the level of the pons may have a negative influence on DTT of the fibers passing through the brainstem. To our knowledge, no study has yet been performed based on the premise that DTT of the pons may require an optimized R factor, which is different from DTT in other brain regions with less geometric distortion, to not only increase the SNR but also decrease the extent of geometric distortion. In this study, DTT of the pyramidal tract passing through the pons was investigated with different R factors. We hypothesized that the calculated fiber number of the tract would be highest in the optimum range of R factors. The SNR, geometric distortion, and the number of fibers visible in the tract were measured to determine the optimal R factor.

MATERIALS AND METHODS

Subjects

This study was approved by the Institutional Review Board, and informed consent was obtained from all subjects. In June 2014, ten healthy volunteers (9 men and 1 woman; median age 30 years, range 27–43 years) were prospectively enrolled in this study. Volunteers had no history of neurologic disease, no current neurologic disease, and no contraindications for MRI scanning.

Imaging Protocol

Diffusion tensor imaging (DTI) was performed at 3 Tesla (In-tera Achieva TX, Philips Healthcare, Best, the Netherlands) using a 32-channel sensitivity encoding (SENSE) head coil. DTI was based on single-shot EPI in the axial plane with the following parameters: b value, 0 and 1000 s/mm²; 15 different directions of diffusion gradients; repetition time (TR), 8888–15000 ms; TE, 118, 80, 67, 60, and 57 ms at R factors 1, 2, 3, 4, and 5; voxel size, 2 × 2 × 2 mm³; slice number, 74. DTI was repeated five times with a different R factor each time (1, 2, 3, 4, and 5). Acquisition times were 5:02, 3:12, 3:09, 3:18, and 3:19 (min:sec) at R factors 1, 2, 3, 4, and 5, respectively.

In order to measure the SNR of DTI with different R factors, a noise map was separately obtained for each subject by a method described in a previous study (16). To measure image distortion, axial T2-weighted turbo spin-echo images were obtained for comparison. The parameters were as follows: TR, 3000 ms; TE, 80 ms; voxel size, 2 × 2 × 2 mm³.

Image Analysis

SNR Measurement

The SNR of EPI (b value, 0 s/mm²) was measured in the cen-

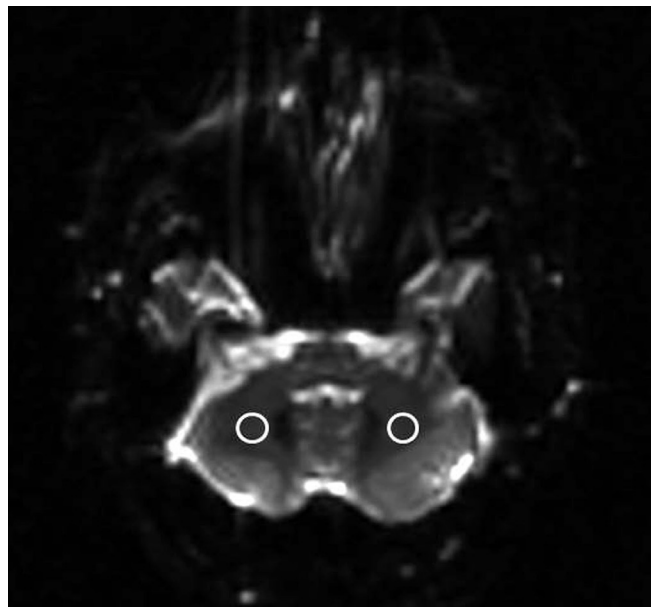


Fig. 1. Measurement of signal-to-noise ratio. Two ROIs are placed on either side of the cerebellar hemisphere on EPI at R factor 1 to measure signal intensities. The measurement was repeated for R factors 2, 3, 4, and 5.

EPI = echo-planar imaging, R = reduction, ROIs = regions of interest

tral portion of the cerebellum rather than in the pons to prevent inaccurate measurements resulting from image distortion of the pons (Fig. 1). First, signal intensities were measured in the right and left cerebellar hemispheres using two regions of interest (ROIs) (53 pixels, area 212 mm²) located just lateral to the dentate nuclei. Then, these two values were averaged to obtain "Signal_{avg}". Next, the noise was measured on a separate noise map, using two ROIs with the same coordinates and areas as those used for the signal measurements in the cerebellum. The measured noise values were also averaged to obtain "Noise_{avg}". Lastly, the SNR was calculated using the equation below (16):

$$\text{SNR} = (\text{Signal}_{\text{avg}} / \text{Noise}_{\text{avg}}) \times (\pi / 2)^{1/2}$$

The SNR measurement described in the three steps above was repeated for R factors of 1, 2, 3, 4, and 5. The SNR at each R factor was then numbered from SNR₁ to SNR₅ and "relative SNR"

was calculated for ease of comparison according to the following equation:

$$\text{Relative SNR}_n = \text{SNR}_n / \text{SNR}_1 \quad (n = 1, 2, 3, 4, 5)$$

Image Distortion Measurement

The degree of image distortion was measured at the level of the pons in the most severely distorted image among consecutive images of axial EPI (Fig. 2). First, the antero-posterior (AP) diameter of the pons was manually measured on T2-weighted turbo spin-echo images as a reference value. Second, the AP diameter of the pons at the same level was measured on each of five EPIs (b value, 0 s/mm²) at R factors of 1, 2, 3, 4, and 5.

For ease of comparison of image distortion, the "relative AP diameter" of the pons for each R factor was calculated as the ratio of the AP diameter on EPI to that on the T2-weighted turbo

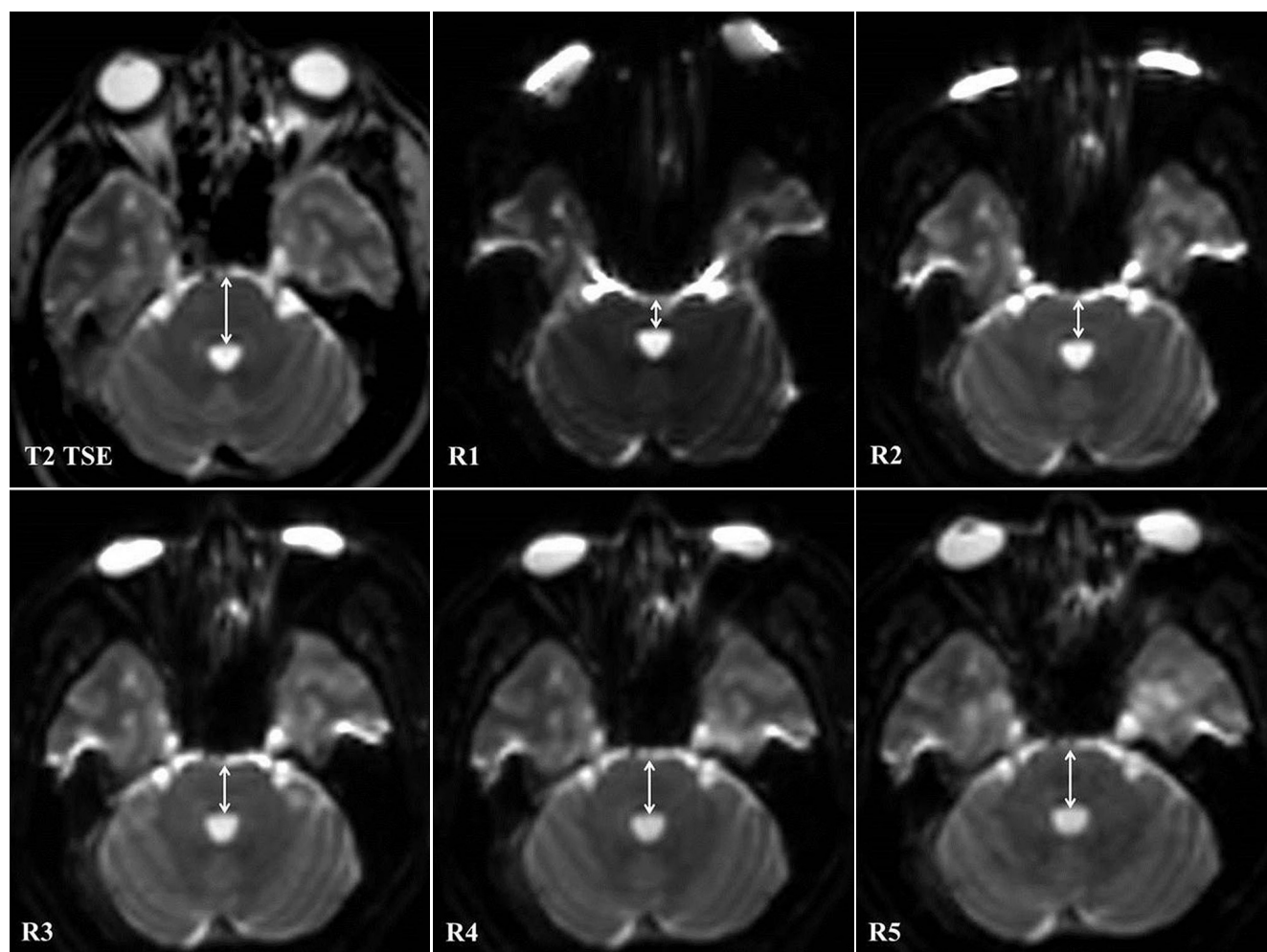


Fig. 2. Measurement of image distortion. Antero-posterior diameter (arrows) of the pons is measured on T2-weighted turbo spin-echo images (T2 TSE) and on EPI at R factors 1, 2, 3, 4, and 5 (R1–5). EPI = echo-planar imaging, R1–5 = reduction factors 1–5

spin-echo image. Therefore, smaller values for the relative AP diameter of the pons indicated stronger image distortion.

Fiber Number Measurement

Fiber tracking was conducted using PRIDE software (Philips Healthcare, Best, the Netherlands) according to a method described in a previous study (17). For the pyramidal tract passing through the pons, two ROIs including the pyramidal tract were located manually on the axial color-coded fractional anisotropy map: the upper ROI was at the cerebral peduncle of the midbrain, and the lower ROI was at the anterior portion of the lower

pons (Fig. 3). Fibers passing through both ROIs were then displayed as a final DTT of the pyramidal tract. Fiber tracking thresholds were set to 0.15 for fractional anisotropy and 27° for the angle between two contiguous eigenvectors. Fiber tracking was performed separately for the right and left pyramidal tracts for all 10 subjects. The fiber numbers of each of the 20 tracts which met the thresholds were then automatically calculated by PRIDE software for R factors of 1, 2, 3, 4, and 5 (Fig. 4).

Statistical Analysis

The Friedman test was used to compare the relative SNR, rel-

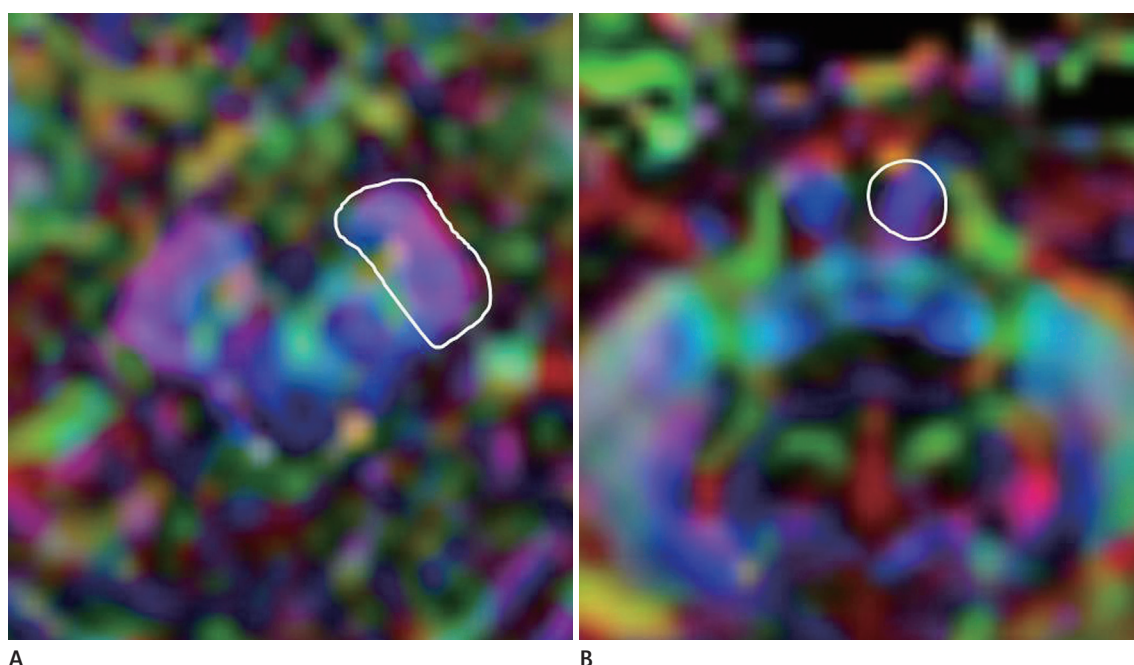


Fig. 3. ROI position for fiber tracking. The upper ROI is placed at the cerebral peduncle of the midbrain (A), and the lower ROI is placed at the anterior portion of the lower pons (B). ROI = regions of interest

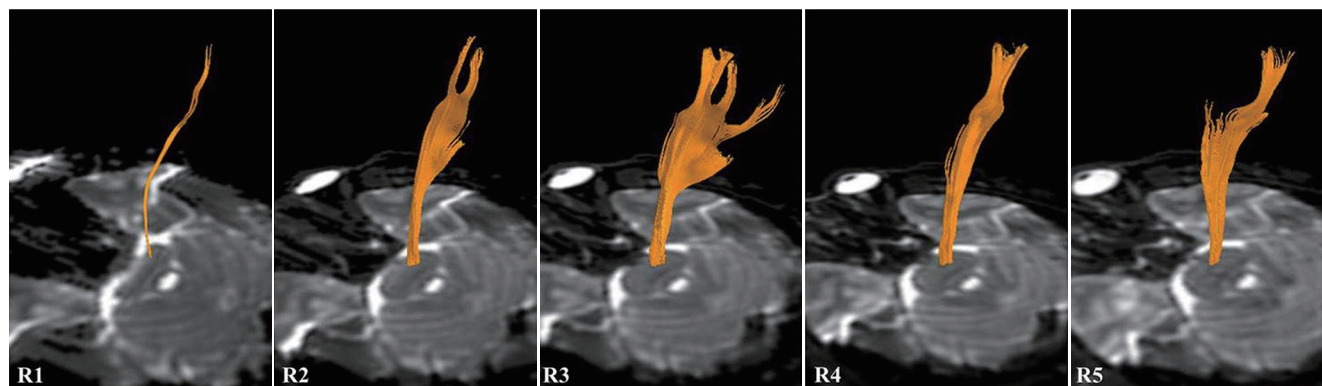


Fig. 4. Fiber tracking of the pyramidal tract. Fiber tracking of the pyramidal tract at R factors 1, 2, 3, 4, and 5 (R1–5) is demonstrated. R1–5 = reduction factors 1–5

Table 1. SNR vs. R Factor ($n = 10$ Subjects)

	Measured SNR					Relative SNR				
	R1	R2	R3	R4	R5	R1	R2	R3	R4	R5
Mean	19.9	23.9	22.0	17.4	9.25	1.00	1.21	1.11	0.88	0.47
SD	2.56	2.03	1.70	1.85	1.24	0	0.13	0.10	0.15	0.08

R1–5 = reduction factors 1–5, SD = standard deviation, SNR = signal-to-noise ratio

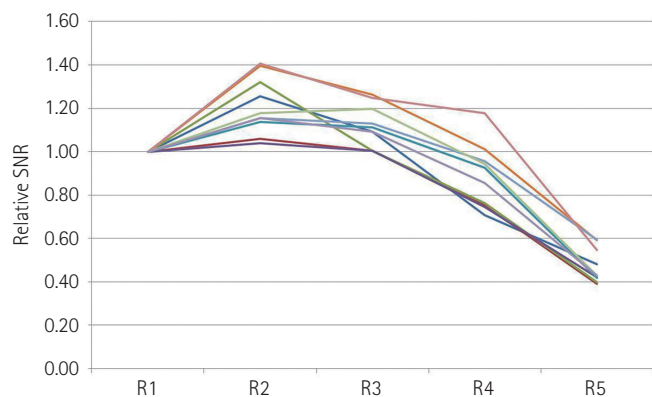


Fig. 5. Relative SNR versus R factor in 10 subjects. Maximal relative SNR is achieved at R factor 2 in 9 subjects. R = reduction, SNR = signal-to-noise ratio

ative AP diameter of the pons, and pyramidal tract fiber number according to the five different R factors. p values less than 0.05 were considered statistically significant. Statistical analysis was performed with the SPSS software package (SPSS, version 18.0; SPSS Inc., Chicago, IL, USA).

RESULTS

SNR

Table 1 shows the SNR results for the 10 subjects. Maximal relative SNR was achieved at R factor 2 in 9 subjects and at R factor 3 in 1 subject (Fig. 5). Relative SNR was significantly different among the five R factors ($p < 0.001$).

Image Distortion

The AP diameters of the pons in all 10 subjects are given in Table 2. Relative AP diameter increased with increasing R factor, which represented monotonically decreasing image distortion with higher R factors. The relative AP diameter was highest at R factor 5 in 9 subjects and at R factor 4 in 1 subject. Relative AP diameters differed significantly among the five R factors ($p < 0.001$).

Fiber Number

The fiber numbers of the right and left pyramidal tracts are given in Table 3. Of 20 tracts from 10 subjects, 11 tracts displayed the largest fiber number at R factor 3, 6 tracts at R factor 4, 2 tracts at R factor 2, and 1 tract at R factor 5. The fiber numbers were significantly different among the five R factors ($p < 0.001$).

DISCUSSION

DTT has proven effective for evaluating several brainstem pathologies (12–15, 18). A previous study (13) reported the reliability of DTT in differentiating between diffuse pontine glioma and brainstem demyelinating disease, in which the fiber tracts of the brainstem are displaced by a tumor but are obscured or even transected by demyelinating disease. DTT has also been used to predict the degree of motor deficit associated with brainstem tumors (12), to assess treatment response in patients with pediatric diffuse brainstem glioma (14, 15), and to plan the surgical approach to brainstem cavernoma by providing information regarding motor and sensory fiber tracts (18). However, it should be noted that DTT is easily compromised by susceptibility-induced geometric distortion, which is an intrinsic shortcoming of EPI (19). The pons is particularly vulnerable to susceptibility artifacts, caused in this case by air in the adjacent sphenoid sinus. Recently, parallel imaging has been integrated into EPI, and has been shown to mitigate the geometric distortion problem (3, 9, 20). The R factor of the parallel imaging process is an important parameter that affects not only the geometric distortion of EPI but also the SNR (7, 8). However, no previous study determined the optimal R factor of parallel imaging for DTT used to visualize fiber tracts in the brainstem.

In this study, we investigated the optimal R factor of parallel imaging for DTT to visualize the pyramidal tract through the pons. Our findings were as follows: first, the SNR proved maximal at R factor 2 and thereafter declined in most of the subjects. This biphasic change of the SNR over the increase in R factor is

Table 2. AP Diameter of the Pons vs. R Factor (*n* = 10 Subjects)

	Measured AP Diameter						Relative AP Diameter					
	R1	R2	R3	R4	R5	TSE	R1	R2	R3	R4	R5	TSE
Mean	12.2	15.9	17.6	18.8	19.3	21.0	0.58	0.76	0.84	0.90	0.93	1.00
SD	2.76	1.80	1.52	1.49	1.41	1.35	0.14	0.09	0.07	0.06	0.06	0

AP = antero-posterior, R1–5 = reduction factors 1–5, SD = standard deviation, TSE = T2-weighted turbo spin-echo image

Table 3. Fiber Number of the Pyramidal Tract vs. R Factor (*n* = 20 Tracts in 10 Subjects)

	Fiber Number				
	R1	R2	R3	R4	R5
Mean	254.3	689.6	899.4	788.3	336.5
SD	311.3	500.9	468.6	546.9	331.7

R1–5 = reduction factors 1–5, SD = standard deviation

supported by several previous studies (3, 7, 8, 21). The SNR increased with the use of higher R factors because of a shortening of the TE (7, 8). However, reconstruction artifacts related to parallel imaging also inevitably increased with increasing R factor (3, 7, 21). Therefore, the maximal SNR, obtained using R factors between 2 and 3 in our study, represents a compromise between the two effects of the R factor (7). Second, the use of a higher R factor reduced image distortion of the pons, resulting in the smallest distortion at R factor 5 in almost all subjects. An increase in the R factor reduces the number of phase-encoding steps per radio frequency shot in EPI (i.e., the EPI factor), which produces a smaller amount of phase error across the phase-encoding direction (3). Therefore, the degree of geometric distortion is less at higher R factors because of mitigation of susceptibility artifacts (9, 10), which was the case in our study. Lastly, the number of fibers in the pyramidal tract was maximal at R factor 3 in the majority of the subjects. An R factor of approximately 3 may therefore provide an optimal balance between SNR and image distortion effects, thereby allowing for visualization of the maximum number of fibers using brainstem DTT. Optimal R factors for DTT at the pons level and for DTT in other brain regions have not been compared. However, we speculate that SNR is a more important factor for DTT in other brain regions where geometric distortion is less than it is in the pons. In our experience, not included in this study, the number of fibers seen in DTT of the pyramidal tract above the pons was maximal at R factor 2, rather than R factor 3, in the majority of subjects.

Our study had some limitations. First, fractional anisotropy and the angle between two contiguous eigenvectors were ad-

opted for thresholding in DTT, following the methods used in many previous studies (12–15, 18, 22). The fiber number of the pyramidal tract could be affected by the particular thresholds used. However, in this study we aimed to compare the relative fiber numbers measured at different R factors, not to determine their absolute values. Thus, our results may not be sensitive to the choice of threshold values. Second, only the fiber number of the pyramidal tract was utilized to assess the outcome of DTT, and other DTI domains such as fractional anisotropy and mean diffusivity were not evaluated. However, we speculate that fractional anisotropy and mean diffusivity must also be affected by the SNR and image distortion. Therefore, our results can likely be expanded to the investigation of other DTI domains in the brainstem in future studies. Third, the presence of individual variation in fiber number, as reported by Reich et al. (23), was not considered in our study. However, the purpose of our study was to evaluate intrasubject differences in fiber number using different R factors, not to assess intersubject differences. Therefore, individual variation will have had little impact on the results of our study. Lastly, our study was conducted using a certain type of MRI system among the many commercially available; therefore, practical application of our methods may not be generalizable to all clinical MRI systems. According to our results, however, the balance between the SNR and image distortion effects should be considered for any type of MRI system used for EPI-based DTT in the brainstem.

In conclusion, R factor 3 is optimal for DTT of the pyramidal tract through the pons. The number of visible fibers in the pyramidal tract was influenced by the combined effect of the SNR and image distortion, which depended on the R factor. A balanced consideration of the SNR and image distortion is necessary for DTT in the pons.

REFERENCES

1. Noël P, Bammer R, Reinhold C, Haider MA. Parallel imag-

- ing artifacts in body magnetic resonance imaging. *Can Assoc Radiol J* 2009;60:91-98
2. Glockner JF, Hu HH, Stanley DW, Angelos L, King K. Parallel MR imaging: a user's guide. *Radiographics* 2005;25:1279-1297
 3. Bhagat YA, Emery DJ, Naik S, Yeo T, Beaulieu C. Comparison of generalized autocalibrating partially parallel acquisitions and modified sensitivity encoding for diffusion tensor imaging. *AJNR Am J Neuroradiol* 2007;28:293-298
 4. Wilson M, Tench CR, Morgan PS, Blumhardt LD. Pyramidal tract mapping by diffusion tensor magnetic resonance imaging in multiple sclerosis: improving correlations with disability. *J Neurol Neurosurg Psychiatry* 2003;74:203-207
 5. Nucifora PG, Verma R, Lee SK, Melhem ER. Diffusion-tensor MR imaging and tractography: exploring brain microstructure and connectivity. *Radiology* 2007;245:367-384
 6. Rollins NK. Clinical applications of diffusion tensor imaging and tractography in children. *Pediatr Radiol* 2007;37:769-780
 7. Jaermann T, Crelier G, Pruessmann KP, Golay X, Netsch T, van Muiswinkel AM, et al. SENSE-DTI at 3 T. *Magn Reson Med* 2004;51:230-236
 8. Jaermann T, Pruessmann KP, Valavanis A, Kollias S, Boesiger P. Influence of SENSE on image properties in high-resolution single-shot echo-planar DTI. *Magn Reson Med* 2006;55:335-342
 9. Blaimer M, Breuer F, Mueller M, Heidemann RM, Griswold MA, Jakob PM. SMASH, SENSE, PILS, GRAPPA: how to choose the optimal method. *Top Magn Reson Imaging* 2004;15:223-236
 10. Morelli JN, Runge VM, Feiweier T, Kirsch JE, Williams KW, Attenberger UI. Evaluation of a modified Stejskal-Tanner diffusion encoding scheme, permitting a marked reduction in TE, in diffusion-weighted imaging of stroke patients at 3 T. *Invest Radiol* 2010;45:29-35
 11. Nagae-Poetscher LM, Jiang H, Wakana S, Golay X, van Zijl PC, Mori S. High-resolution diffusion tensor imaging of the brain stem at 3 T. *AJNR Am J Neuroradiol* 2004;25:1325-1330
 12. Lui YW, Law M, Chacko-Mathew J, Babb JS, Tuvia K, Allen JC, et al. Brainstem corticospinal tract diffusion tensor imaging in patients with primary posterior fossa neoplasms stratified by tumor type: a study of association with motor weakness and outcome. *Neurosurgery* 2007;61:1199-1207; discussion 1207-1208
 13. Giussani C, Poliakov A, Ferri RT, Plawner LL, Browd SR, Shaw DW, et al. DTI fiber tracking to differentiate demyelinating diseases from diffuse brain stem glioma. *Neuroimage* 2010;52:217-223
 14. Prabhu SP, Ng S, Vajapeyam S, Kieran MW, Pollack IF, Geyer R, et al. DTI assessment of the brainstem white matter tracts in pediatric BSG before and after therapy: a report from the Pediatric Brain Tumor Consortium. *Childs Nerv Syst* 2011;27:11-18
 15. Khatua S, Hou P, Bodiwala R, Wolff J, Hamilton J, Patil S, et al. Preliminary experience with diffusion tensor imaging before and after re-irradiation treatments in children with progressive diffuse pontine glioma. *Childs Nerv Syst* 2014;30:925-930
 16. Gudbjartsson H, Patz S. The Rician distribution of noisy MRI data. *Magn Reson Med* 1995;34:910-914
 17. Mori S, Crain BJ, Chacko VP, van Zijl PC. Three-dimensional tracking of axonal projections in the brain by magnetic resonance imaging. *Ann Neurol* 1999;45:265-269
 18. Ulrich NH, Kockro RA, Bellut D, Amaxopoulou C, Bozinov O, Burkhardt JK, et al. Brainstem cavernoma surgery with the support of pre- and postoperative diffusion tensor imaging: initial experiences and clinical course of 23 patients. *Neurosurg Rev* 2014;37:481-491; discussion 492
 19. Merhof D, Soza G, Stadlbauer A, Greiner G, Nimsch C. Correction of susceptibility artifacts in diffusion tensor data using non-linear registration. *Med Image Anal* 2007;11:588-603
 20. Bammer R, Auer M, Keeling SL, Augustin M, Stables LA, Prokesch RW, et al. Diffusion tensor imaging using single-shot SENSE-EPI. *Magn Reson Med* 2002;48:128-136
 21. Deshmene A, Gulani V, Griswold MA, Seiberlich N. Parallel MR imaging. *J Magn Reson Imaging* 2012;36:55-72
 22. Lee JS, Han MK, Kim SH, Kwon OK, Kim JH. Fiber tracking by diffusion tensor imaging in corticospinal tract stroke: topographical correlation with clinical symptoms. *Neuroimage* 2005;26:771-776
 23. Reich DS, Smith SA, Jones CK, Zackowski KM, van Zijl PC, Calabresi PA, et al. Quantitative characterization of the corticospinal tract at 3T. *AJNR Am J Neuroradiol* 2006;27:2168-2178

뇌간 추체로의 확산텐서 신경다발 영상: 병렬 영상에서의 적정 감소 인자에 대한 연구

배운정 · 박종빈 · 김재형* · 최병세 · 정철규

목적: 병렬영상의 감소 인자 선택은 자화율 인공물을 변화시켜 뇌교의 확산텐서 신경다발 영상에 영향을 미치므로 뇌교 추체로의 섬유 개수를 최대로 표현할 수 있는 감소 인자를 찾고자 하였다.

대상과 방법: 10명의 건강한 사람들을 대상으로, single-shot 에코평면영상기법의 확산텐서 영상을 시행한다. 영상 파라미터는 b value 1000, 경사방향 15, 복셀, $2 \times 2 \times 2 \text{ mm}^3$, 감소 인자, 1, 2, 3, 4, 5로서 10명의 뇌교에서 좌우 총 20개의 추체로 신경다발 영상을 얻었다. 신호대잡음비, 영상 왜곡, 그리고 섬유 개수를 감소 인자에 따라 비교하였다.

결과: 신호대잡음비, 영상 왜곡, 섬유 수는 감소 인자에 따라 유의한 차이를 보였다. 신호대잡음비는 감소 인자 2에서 가장 높았고, 영상 왜곡은 감소 인자 5에서 가장 낮았다. 섬유 개수는 감소 인자 3에서 가장 많았다.

결론: 뇌교 추체로의 확산텐서 신경다발 영상에서 최적의 감소 인자는 3으로 생각된다. 신호대잡음비와 영상 왜곡은 감소 인자에 대한 종속도가 다르므로 뇌교의 신경다발 영상을 시행할 때 두 변수 사이의 균형적인 고려가 필요하다.

서울대학교 의과대학 분당서울대학교병원 영상의학과학교실